Journal of Power Sources 381 (2018) 30–37

Contents lists available at ScienceDirect

Journal of Power Sources

journal homepage: www.elsevier.com/locate/jpowsour

Power ramp rate capabilities of a 5 kW proton exchange membrane fuel cell system with discrete ejector control

K. Nikiforow*, J. Pennanen, J. Ihonen, S. Uski, P. Koski

VTT Technical Research Centre of Finland Ltd, P.O. Box 1000, FI-02044 VTT, Finland

HIGHLIGHTS

- Ejector-based PEMFC system power ramp-rate capabilities were studied.
- Fuel supply manages a 50%–100% power ramp in 0.1 s even in low-volume systems.
- Air supply with 2.5 initial stoichiometry manages a 50%–93% power ramp in 1.0 s.
- Air supply with 7.0 initial stoichiometry manages a 50%–93% power ramp in 0.1 s.

ARTICLE INFO

Keywords:
PEMFC system
Power ramp rate
Dynamic behavior
Ejector
Fuel supply
Air supply

ABSTRACT

The power ramp rate capabilities of a 5 kW proton exchange membrane fuel cell (PEMFC) system are studied theoretically and experimentally for grid support service applications.

The fuel supply is implemented with a fixed-geometry ejector and a discrete control solution without any anode-side pressure fluctuation suppression methods. We show that the stack power can be ramped up from 2.0 kW to 4.0 kW with adequate fuel supply and low anode pressure fluctuations within only 0.1 s.

The air supply is implemented with a centrifugal blower. Air supply ramp rates are studied with a power increase executed within 1 and 0.2 s after the request, the time dictated by grid support service requirements in Finland and the UK. We show that a power ramp-up from 2.0 kW to 3.7 kW is achieved within 1 s with an initial air stoichiometry of 2.5 and within 0.2 s with an initial air stoichiometry of 7.0. We also show that the timing of the power ramp-up affects the achieved ancillary power capacity.

This work demonstrates that hydrogen fueled and ejector-based PEMFC systems can provide a significant amount of power in less than 1 s and provide valuable ancillary power capacity for grid support services.

1. Introduction

Proton exchange membrane fuel cells (PEMFCs) are seen as a valid alternative to diesel generators in backup power and grid balancing applications both in the kW- and MW-range. The main advantages of a PEMFC in these applications are start-up reliability, low start-up costs, ability to respond rapidly to load changes, zero local emissions, and low noise level.

The need for backup power and grid balancing services increases with the amount of variable renewable energy (VRE) in the grid. In particular, the inherent inertia of the system decreases as the penetration of conventional synchronous generators decreases in power systems [1]. The decrease in inertia is mainly due to increasing wind and photovoltaic (PV) solar power generation or electricity imports via high voltage direct current (HVDC) links.

Decreased inertia deteriorates the stability of the power system in case of disturbances. Inertia determines the lowest momentary frequency occurring within a few seconds after a major system frequency disturbance, which typically is caused by the loss of a large power plant or significant transmission connection.

The decrease of inherent inertia can be offset in a number of ways, e.g., keeping a sufficient amount of synchronous generation online in the system and thus curtailing non-synchronous generation or limiting imports via HVDC connections, adding rotating masses like synchronous condensers into the system, or establishing a market for inertia and thus promoting implementation of synthetic inertia. Synthetic inertia could be obtained from non-synchronous units (e.g., wind power plants, solar PV, batteries) by modulating the power output in a manner similar to how synchronous units provide power as inertial response [2]. In Europe, transmission system operators (TSOs) could require non-

* Corresponding author.
E-mail address: kaj.nikiforow@vtt.fi (K. Nikiforow).

https://doi.org/10.1016/j.jpowsour.2018.01.090
Received 1 September 2017; Received in revised form 26 January 2018; Accepted 30 January 2018
Available online 08 February 2018

synchronous Power Park Modules (PPM) to be capable of providing synthetic inertia. This requirement could be applied to PPMs with capacities of a few to tens of megawatts and above depending on the synchronous system [3,4]. Neither inertia requirements nor inertia as an ancillary service is yet widely used.

Inertia is related to the rate of change of frequency (RoCoF) immediately after a disturbance. Frequency containment disturbance reserves (FCR-D) determine the following steady frequency [2,5]. Frequency indicates the balance between system load and power generation and, thus, both power generation and loads can be used for FCR-D.

Historically, load shedding – i.e. fast tripping of loads – has been the means for rapid handling of severe low frequency disturbances due to loss of power supply. In Finland, for example, a tendering for load shedding is employed for system protection because of to the 1600 MW nuclear power production unit that is expected be online in 2019 and will affect the Nordic power system operation security.

In the UK's Enhanced Frequency Response (EFR) market [6], reserve capacity must be activated fully within 1 s and be able to sustain support for a minimum 15 min. Batteries have proven to be a very cost effective way to provide a fast response in the UK EFR tender. The feasibility and applicability of similar fast frequency response systems has been investigated by local authorities, e.g. in Australia [7] and in Texas, U.S [8].

In addition to load shedding and batteries, system protection and EFR could also be implemented by fast generation control reserves with similar control characteristics, i.e., an ability to provide power within 1 s. This creates a new opportunity for fuel cells and, in particular, for PEMFCs, which can achieve a very high power ramp rate.

In Finland, a significant amount of hydrogen is produced as a by-product in chlorine and sodium chlorate factories [9], and the quality of that hydrogen is sufficient for use as fuel in PEMFCs [10]. Using this hydrogen in PEMFC power plants operating at partial load, a significant rapid load response could be provided. However, the ability of PEMFC power plants to provide this ancillary service should be proven by verifying their power ramp rate capability.

A number of factors limit the power ramp rate of hydrogen fueled PEMFC systems, including air supply, fuel supply, and power electronics. These limitations are dependent on the system design and operation. Therefore, the power ramp rate capability can be improved by optimizing the system design and operation.

Air supply is well known to limit the power ramp-up rate in PEMFC systems. In principle, there are three issues: the dynamic capability of the blower/compressor, the gas manifold volume, and the time lag of the control system. Corbo et al. analyzed a 20 kW_e PEMFC system using different air supply strategies. By applying excess air at low loads, a 20%/s power ramp rate was achieved [11]. However, the use of excess air flow rate reduces system efficiency by adding blower power consumption and increases system cost through the need of a more efficient humidifier. In another study, Corbo et al. showed that 10%/s power ramp rate is possible (with minor issues) starting from room temperature [12]. Danzer et al. studied and modeled the control of cathode air excess and pressure in a pressurized PEMFC, showing that with an observer-based multivariable control, a 50%/s power ramp rate is possible [13]. However, the inertia of the compressor was not considered because a mass flow controller supplied the air. The study of Danzer et al. also illustrates that maintaining the cathode pressure close to set-point might be challenging during transients. In pressurized systems, not only does the cathode pressure need to be controlled but also the anode pressure, thus adding complexity. Matraji et al. studied the control of a compressor by modeling and employing a Hardware-In-Loop test bench [14]. According to their results, it takes up to 9 s to increase the air flow rate from 0 to 100%. This long duration may be due to the high inertia of the twin-screw compressor and the limited power of a compressor motor. Based on the literature study, at least a 20–30%/s power ramp rate is possible without extra measures at the air supply side.

The fuel supply also limits the power ramp rate, especially when the system is pressurized and an ejector is employed for anode gas recirculation. In a pressurized system, the anode pressure needs to be controlled to avoid a too high pressure difference over the membrane, leading to possible limitations in power ramp rate. When an ejector is applied, the ejector primary pressure control will further complicate the management of the anode pressure, especially if discrete flow control is applied [15]. Anode gas recirculation is applied in PEMFC systems for fuel humidification and to avoid local fuel starvation [16,17].

A third limitation for the power ramp rate is the thermal management, especially when the stack power density is high. The power densities of present day PEMFC stacks are in the range of 3 kW/dm^3 [18]. When the power is increased from the minimum to the maximum level, the cooling demand may increase up to 5 kW per kilogram of stack mass. This would lead to a temperature increase rate of 2–4 °C/s.

The transients in reactant supply or temperature can also lead to severe degradation of the catalyst layer, as reviewed by e.g. Banerjee [19]. Pei and Chen have reviewed the main factors affecting the lifetime of PEMFC in vehicle applications, and reactant starvation during fast transients is one of the issues [20].

To date, PEMFC systems hydrogen fuel ramp rate capabilities have not been studied, only the air supply capabilities. In addition, in these air supply studies, the focus has been on the time scale of several seconds, not 0.2–2 s, which are needed in many applications, including ancillary services for TSOs.

The present work studies the hydrogen fuel supply ramp rate capabilities of a PEMFC system with an ejector with discrete control. The capabilities of an ejector-based system are studied for the first time without using any anode pressure fluctuation mitigation methods during the transient, such as anode purge [15]. In addition to the fuel supply, the air supply ramp rate capabilities are studied. The work focuses on determining the maximum power increase achievable with a PEMFC system operated at partial load, with the power increase executed within 0.2 or 1–2 s after the request, as suggested by the requirements for ancillary power applications.

2. Methods

2.1. PEMFC system description

Fig. 1 shows the simplified schematic of the PEMFC system employed in this work. The fuel was supplied through a fixed-geometry ejector (E), employed for anode gas recirculation. The ejector primary pressure was controlled using a setup of three solenoid valves and three flow restrictors (EPC), enabling fuel supply at seven discrete flow rates. The fuel supply in the present setup limits the maximum PEMFC power to approximately 4 kW. The load current was fine-tuned to compensate for the possible small variation in fuel supply rate and to maintain a constant anode pressure during steady state operation. Air was supplied with a blower (B) and humidified with a membrane humidifier (MH). A coolant pump (P) recirculated de-ionized water through the stack and through a liquid-liquid heat exchanger (HEX). The PEMFC system was controlled with National Instruments CompactRIO hardware, which was programmed with LabVIEW software. A complete description of the system can be found in previous work [15].

The control software was adopted for the current work, firstly by a higher data acquisition rate (100 Hz), which was triggered prior to a power transient and maintained for 10 s. Secondly, the experiments conducted in this work – the study of system ramp rate capabilities and the control of anode pressure during power transients – relied on exact timing of the fuel valve (in EPC), the air blower, and the electronic load control. Therefore, the control routine was updated to achieve accurate control, with the timing error of 1 ms or below.

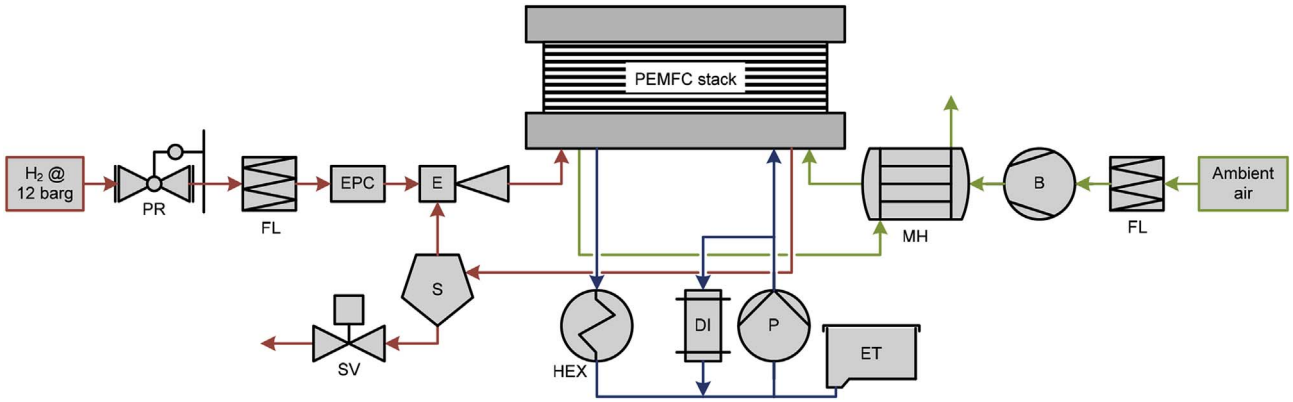

Fig. 1. Simplified PEMFC system scheme. PR: pressure reducer, FL: particle filter, EPC: ejector primary pressure control, E: ejector, BV: buffer volume, S: gas-liquid separator, SV: solenoid valve, B: gas blower, MH: membrane humidifier, P: liquid pump, DI: de-ionizing filter, HEX: liquid-liquid heat exchanger, ET: expansion tank.

2.2. Anode pressure control during power transients

The discrete ejector control has been shown to be a viable solution to achieve fast power ramp rates [15]. A challenge with this solution, however, is to maintain the balance between the hydrogen fuel supply and consumption rate at all times in order to avoid excessive anode pressure fluctuation. The imbalance between fuel supply and consumption can be mitigated by either increasing the anode gas volume or using a long anode purge during the transient.

However, both of these mitigation alternatives have clear drawbacks. Increasing the anode volume will increase the gas exchange time during a system start-up, causing additional degradation [21]. For this reason, a minimum anode volume is preferred. A long anode purge during operation depressurizes the anode side and causes a pressure difference between the anode and cathode, causing unnecessary stresses for the polymer membrane [22]. A long anode purge also causes extra fuel consumption.

It is, therefore, important to study alternative methods for mitigating anode pressure fluctuations that require neither extra anode gas volume nor extra anode gas purging. Precise control of fuel supply timing relative to the load ramp-up is recognized as one such method. Since experimental studies of this approach could damage the system and endanger personal safety, simulations were conducted for the initial study and to assist in designing the system.

The anode gas volume in the current system was measured to be 1.5 dm^3 [15] – a relatively large value compared to the nominal power and current of system (5 kW, 200 A and 50 cells). Thus, the anode volume-to-power ratio for the current system is 0.3 dm^3/kW. A 10 A mismatch in fuel supply and consumption rates leads to only approximately 40 mbar/s pressure change rate in this system. In volume-optimized systems, the anode volume-to-power ratio can be as low as 0.06 dm^3/kW and the corresponding pressure change rate can be 5 times faster. When the mismatch between fuel consumption rate and supply increases (e.g., during load changes), the rate of pressure change can be notably higher and actions must be taken within a fraction of a second.

2.3. Fuel supply modeling

A model for studying the anode dynamics was implemented in Mathworks Simulink employing the thermodynamic function library Thermolib by EUtech Scientific Engineering GmbH. The modeled system was based on the experimental system presented in section 2.1 and comprised three parts: the ejector, the PEMFC stack, and the recirculation loop (Fig. 2).

The ejector was modeled with a lookup table based on experimental data [23]. The ejector's secondary gas flow rate was calculated in the 'Ejector' block based on the primary gas pressure and the pressure difference between ejector outlet and secondary inlet. The ejector primary gas pressure was calculated in the 'Control unit' block, and it was dependent on the combination of valves opened. The control signals for valves were modeled as step functions and they were generated in the 'Control signals'-block. The change of ejector primary pressure (p_p) between two discrete load levels was modeled with a transfer function shown in Fig. 3.

The stack model (implemented in the 'Stack'-block) was based on a PEMFC model-block provided in Thermolib. Essential functionalities of the model were 1) fuel consumption, which was proportional to the load current, and 2) the addition of water due to water transport. During simulations, the stack operating temperature was set at 70 °C and the cathode was fed with air at a stoichiometric ratio of 4.

The 'Recycling' block split the flow into recirculated stream and purged stream in case the purge valve was open. In this study, the anode purge was not employed and the 'Recycling'-block simply recirculated the anode gas to the ejector secondary inlet.

The three model blocks 'Ejector', 'Stack', and 'Recycling' had their specified volumes that, together with in- and out-flow rates, determined their pressure levels. The in- and out-flow rates were determined based on the block pressure levels and flow restrictions between them. The flow restrictions were tuned to correspond to pressure drops in the real system.

The stack load current was fine-tuned with a PI-controller in order to maintain a constant anode pressure. A similar functionality was employed in the real system with the exception that the PI-control was disabled during the transient to better observe the anode pressure behavior.

2.4. Experimental procedure

The experiments were conducted by operating the PEMFC at constant load current (approximately 55 A) with load fine-tuning enabled until a steady state was reached. At this point, the load fine-tuning was disabled, the fast data acquisition was triggered, a ramp-up control sequence was applied, and the load current was increased to approximately 160 A. The PEMFC system operating parameters are listed in Table 1 and the ramp-up control sequences are described below.

Three control sequences were applied for studying fuel supply and air supply ramp rates. A control sequence in this context comprises the initiation of fuel supply ramp, air supply ramp, and load ramp at specified moments in time. In each control sequence, the timing of control actions were varied. Table 2 summarizes each control sequence and more detailed descriptions are given below.

The control sequence named as 'Fuel supply' was employed for studying the fuel supply ramp rate. The timing of load ramp-up relative to the fuel supply ramp-up (t_{lrf}) was varied between −50 ms and +200 ms. The timing of air blower ramp relative to the fuel supply

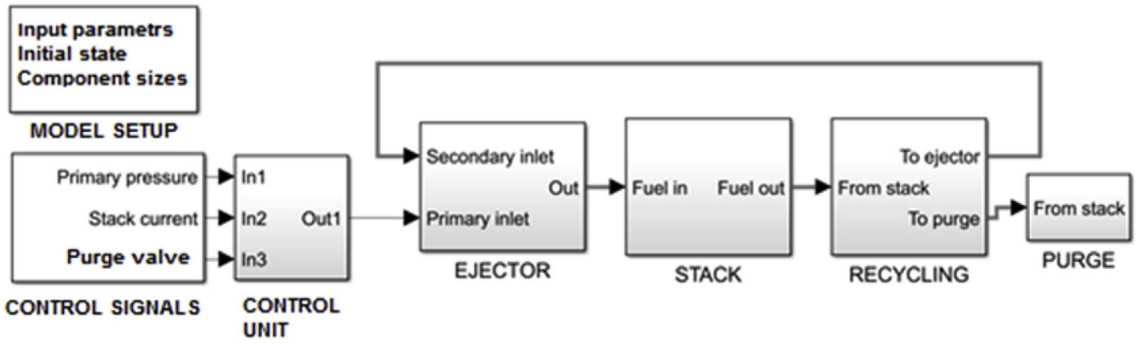

Fig. 2. System model block diagram.

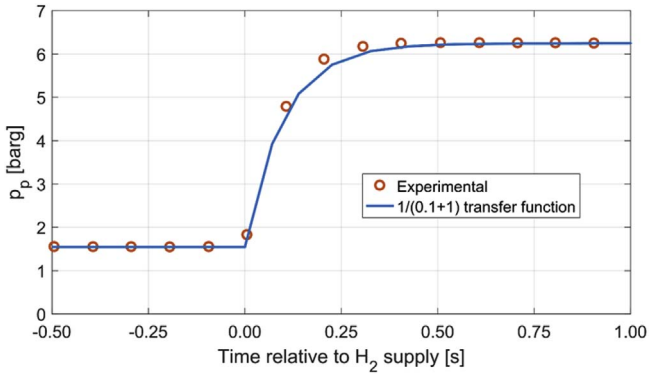

Fig. 3. Measured and modeled transition between two ejector primary pressure (p_p) levels.

Table 1
System operating parameters.

Operating parameter	Target value
Stack current (low power)	55 A (P_{stack} = ~2 kW)
Stack current (high power)	160 A (P_{stack} = ~4 kW)[a]
Anode inlet pressure	0.1 barg
Air stoichiometry	2.5
Coolant inlet temperature	70 °C
Coolant flow rate	~20 lpm

[a] The maximum stack current, 200 A [24], could not achieved because of the ejector control system sizing [15].

Table 2
Control sequence during transients with varying advance in fuel supply, varying advance in air supply, and varying initial air stoichiometry.

Action	Relative time [ms]		
	Fuel supply	Air supply for 1.0 s target	Air supply for 0.2 s target
Increase air stoichiometry	not used	not used	−5000
Initiate air blower ramp-up	−2000	0	0
Initiate fuel supply ramp-up	0	+250, +500, +750, +1000, +1250, +1500, +2000	0
Initiate load ramp-up	−50, 0, +50, +100, +200	+350, +600, +850, +1100, +1350, +1600, +2100	+100

ramp was kept constant at −2.0 s, thereby eliminating the effect of air supply.

The control sequence labeled 'Air supply for 1.0 s target' was employed for studying the maximum achievable power increase within about 1 s. In this sequence, the load ramp-up relative to the air blower ramp-up (t_{tra}) was varied and the initial air stoichiometry was kept at 2.5. The fuel supply ramp was initiated at −100 ms relative to the load ramp because this timing was shown to provide minimum anode pressure fluctuation.

The control sequence labeled 'Air supply for 0.2 s target' was employed for studying the maximum achievable power increase within 0.2 s. This case corresponds to a grid balancing application after a disconnection of a large power unit or import power line. Using this short delay, the initial air stoichiometry was varied between 4.0 and 7.0. The fuel supply ramp was initiated simultaneously with the air blower ramp-up. The load was ramped up 100 ms later. The rest of the 0.2 s target time, i.e., 100 ms, was reserved for the response time of the data transfer and control system in the application.

Each control sequence was repeated 5 to 7 times with each set of parameters, with the exception of experiments that resulted in a deep voltage dip during the transient (experiments with too little time for blower acceleration or too low initial air stoichiometry). These experiments could be conducted only 1 or 2 times because of the control system triggering an emergency shutdown.

3. Results and discussion

3.1. System transient behavior

Fig. 4 displays the high repeatability of measured quantities during seven repetitions of a power transient conducted with the air blower ramp initiated −2000 ms and the load ramp initiated +100 ms relative to the fuel supply ramp-up. These results represent well all measurements in this work.

As seen in Fig. 4a, the load current changes so rapidly that current ramp cannot be captured with the 100 Hz measuring frequency. On the contrary, the stack voltage (Fig. 4b) does not respond instantly to increased current. This results in power peak during the transient, which is followed by a power dip (Fig. 4c). The current increase seen approximately 1 s after the transient is caused by the activation of load fine-tuning.

Compared to the load current ramp, the fuel supply and the air supply ramps are slow. The hydrogen fuel pressure at ejector primary inlet develops in less than 0.5 s (Fig. 4e), while the blower requires approximately 1.5 s for accelerating to the target flow rate (Fig. 4g). The air stoichiometry is computed from the air flow rate and the load current and, thus, changes abruptly with the load current (Fig. 4h).

Fig. 4d shows how the cooling liquid temperature increases after the load change. The stack used in this system (PowerCell S2) is not as volume optimized as automotive stacks. Nonetheless, the coolant outlet temperature increases by 3 °C in 4 s, even though the load change is only 40% of the maximum stack power. In automotive stacks, the rate of change in stack power relative to stack thermal mass can be up to ten

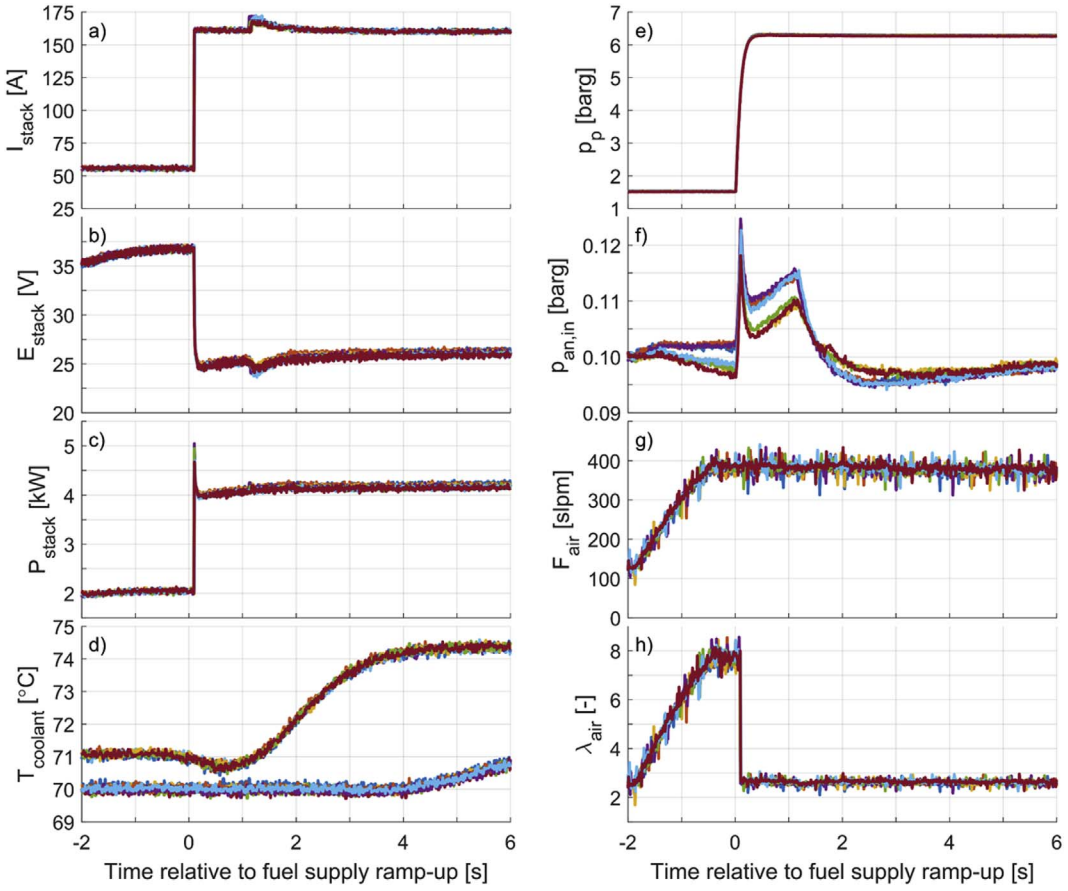

Fig. 4. a) Stack current (I_{stack}), b) stack voltage (E_{stack}), c) stack power (P_{stack}), d) coolant inlet and outlet temperatures ($T_{coolant}$), e) ejector primary inlet pressure (p_p), f) anode inlet pressure ($p_{an,in}$), g) cathode inlet dry air flow rate (F_{air}), and h) air stoichiometry (λ_{air}) during seven repeated transients with air blower ramp-up performed −2000 ms and load ramp-up performed +100 ms relative to hydrogen supply ramp-up.

times larger. This implies a clear risk of stack overheating, unless a feed-forward control method is applied for regulating the coolant flow rate and radiator cooling power.

The variation in anode pressure between experiments (Fig. 4f) is due to disabling the load current fine-tuning at time −2 s relative to the fuel supply ramp-up. From this point on, the anode pressure is not controlled and its value depends on the last load current value. Because of this, the anode pressure relative to the pressure in the beginning of transient ($p_{relative}$) is employed from now on for easier comparison of results. The variation in anode pressure does not affect the fuel supply rate because the flow at the ejector primary nozzle is critical at both current levels employed [15].

3.2. Fuel supply ramp rate

The modeled relative anode pressure profiles ($p_{relative}$) with varying load ramp timings with respect to the fuel supply ramp-up (t_{lrf}) are shown in Fig. 5a. As seen, there is always an anode under- or over-pressurization, or both. This is because the fuel consumption rate changes almost instantaneously with the load current, while the change in fuel flow rate is slower. After the load ramp-up, the pressures in all cases start to approach zero relative pressure because of the load current fine-tuning.

Fig. 5b shows the minimum and maximum simulated relative anode pressure as a function of t_{lrf}. The minimum pressure variation of 24 mbar (−11 to +13 mbar) is achieved with t_{lrf} = +80 ms. With t_{lrf} = +100 ms, the pressure variation is −5 to +19 mbar. If the anode gas volume were to decrease to one fifth, the pressure variation would be five times larger, about 120 mbar. In the current system, a t_{lrf} as low as −100 ms or as high as +200 ms does not cause severe anode pressure fluctuation. Thus, these simulation results were used as reference when planning the experimental part.

The effect of t_{lrf} on anode pressure variation measured experimentally is shown in Fig. 6d. The experimental results accord well with simulated data. Out of the five tested load ramp-up timings, the smallest anode pressure variation of 21 mbar (0 to +21 mbar) was measured with t_{lrf} = +100 ms.

Fig. 6a shows that the minimum stack voltage during transients decreases progressively with decreasing t_{lrf}. All measurements fit this trend perfectly, apart from the sequence with t_{lrf} = +100 ms, which is offset from other measurements by a few hundred millivolts. Nonetheless, ramping up the load as early as 50 ms before initiating the fuel supply (t_{lrf} = −50 ms) does not result in a notable voltage dip. This is because the anode volume functions as a fuel buffer. Hence, a smaller anode volume would presumably result in a more notable voltage dip. However, a smaller anode volume would also result in a higher anode pressure fluctuation, as discussed above. By comparing the anode pressure data and stack voltage data, it can be concluded that the t_{lrf} should be adjusted mainly based on the allowed anode pressure fluctuation.

Because of the small variation in minimum stack voltage between measurements, the minimum stack power also has only small variances (Fig. 6b) – with t_{lrf} = +100 ms the minimum power is 4.0 kW and with all other t_{lrf} the minimum power is 3.9 kW. Thus, the fuel supply can achieve a power ramp-up from 2.0 kW to at least 3.9 kW (a 48% power increase relative to maximum power) in −0.05 to +0.2 s relative to the fuel supply ramp-up.

Fig. 6d shows that a t_{lrf} of +50 ms or less results in anode under-

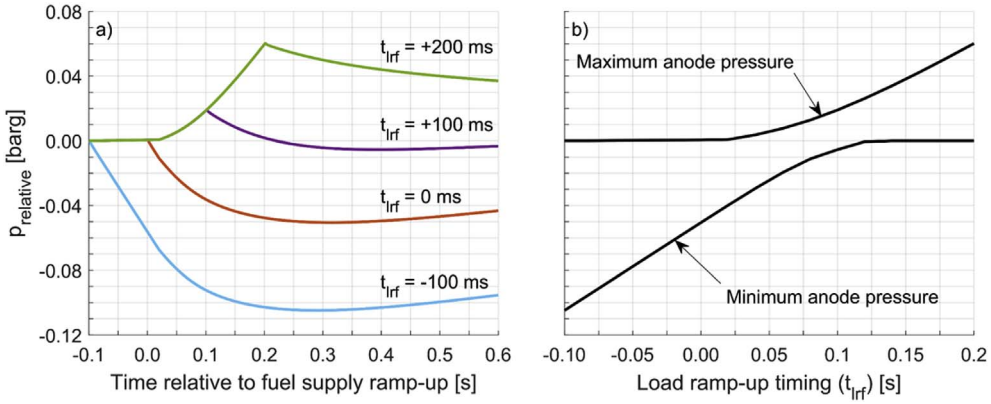

Fig. 5. a) Simulated relative anode pressure ($p_{relative}$) during transients with varying load ramp-up timing relative to fuel supply ramp-up (t_{lrf} = −100 ms…+200 ms). b) The minimum and maximum anode pressure during transients with varying load ramp-up timing relative to fuel supply ramp-up.

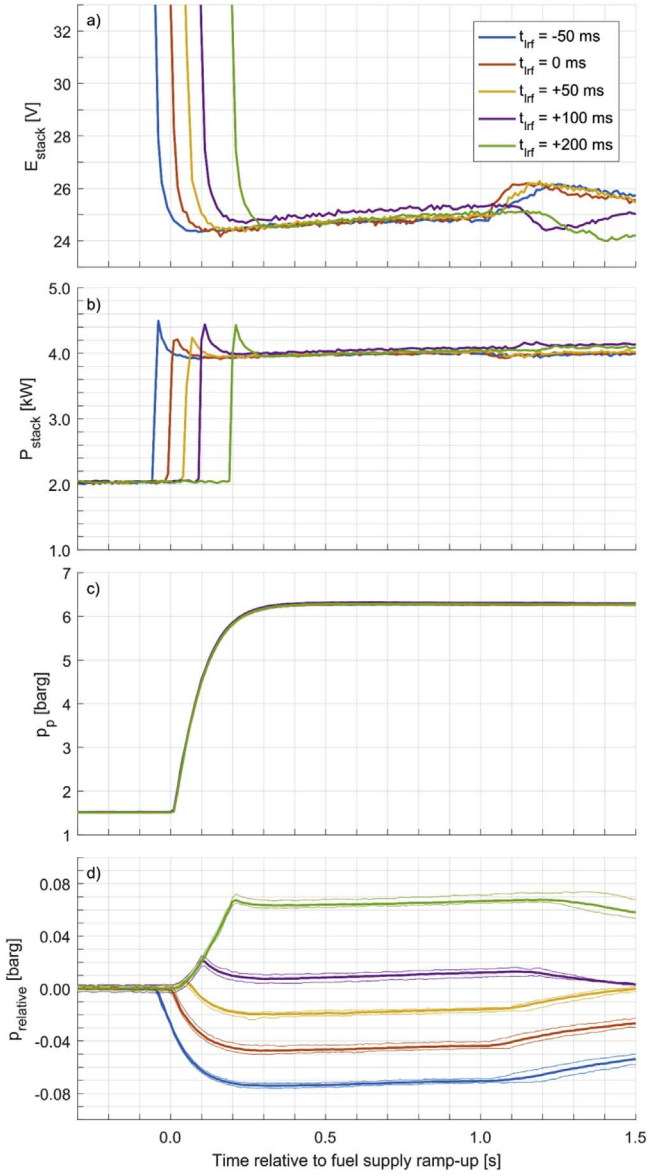

Fig. 6. a) Stack voltage (E_{stack}), b) stack power (P_{stack}), c) ejector primary inlet pressure (p_p), and d) relative anode pressure ($p_{relative}$) during transients with varying load ramp-up timing relative to fuel supply ramp-up (t_{lrf} = −50 ms…+200 ms). The thin lines in figure d show the measured variation in anode pressure between repeated experiments.

pressure. Consequently, when the load fine-tuning is activated, the load current decreases, which results in reduced stack power. This decreases the ancillary power capacity available for sale to the TSO. Therefore, the load ramp-up timing should be chosen to create anode over-pressure, in this case t_{lrf} = +100 ms or t_{lrf} = +200 ms.

The reproducibility of these experiments is very high – the highest and lowest anode pressures measured at the time of load ramp-up in each control sequence in Fig. 6d show a maximum variation of 8 mbar. This indicates that the variation in the opening time of the valves is very small: in the order of 10 ms. A similar conclusion can be made when comparing the evolution of ejector primary pressures after the initiation of fuel supply in Fig. 6c. This low timing variation would be acceptable even in volume-optimized systems using the maximum load step.

3.3. Air supply ramp rate

3.3.1. Varying air blower ramp-up timing for a 1.0 s response

In the studied application, the ancillary power capacity delivered after 1 s forms the basis for the payment from the TSO. Fig. 7 shows the power capacity measured with fixed initial air stoichiometry ($\lambda_{air,0}$ = 2.5) and varying load ramp-up timing relative to the air blower ramp-up (t_{lra}) – not relative to fuel supply ramp-up as in the previous section.

Fig. 7b shows that the earlier the load is ramped up, the higher is the ancillary power capacity. This is contradictory to what could be expected if the stack power is assumed reactant mass transfer limited because the earlier the load is ramped up, the lower is the oxygen concentration at the cathode until a steady state is reached. The observed behavior is believed to be due to water formation at the cathode, the water humidifying the membrane and decreasing resistive losses.

Consistent with the observation of higher stack power with an earlier load ramp-up, the highest stack power (3.7 kW) 1 s after the air blower ramp-up is achieved with a power ramp-up initiated 350 ms after the air blower ramp-up. The power increase corresponds to about 43% of the maximum power. The minimum air stoichiometry during this power transient is 1.2, as seen in Fig. 7c, and a much earlier current ramp-up would result in air under-stoichiometry.

An earlier power ramp-up does not always result in higher power at a given instant. For example, if the target time for the ancillary power is 0.6 s after the trigger, a power ramp-up executed at that very instant or few milliseconds earlier would result in higher power capacity than a power ramp-up executed 350 ms after the trigger, as seen in Fig. 7b. It is concluded that an earlier power ramp-up is beneficial only if it can be performed early enough for the water formation to affect membrane performance. Based on the results shown in Fig. 7b, the time needed for water formation to have an effect is approximately 0.5 s.

The PEMFC system operation should be designed based on lowest performing cell because, at least in typical systems, this will trigger the

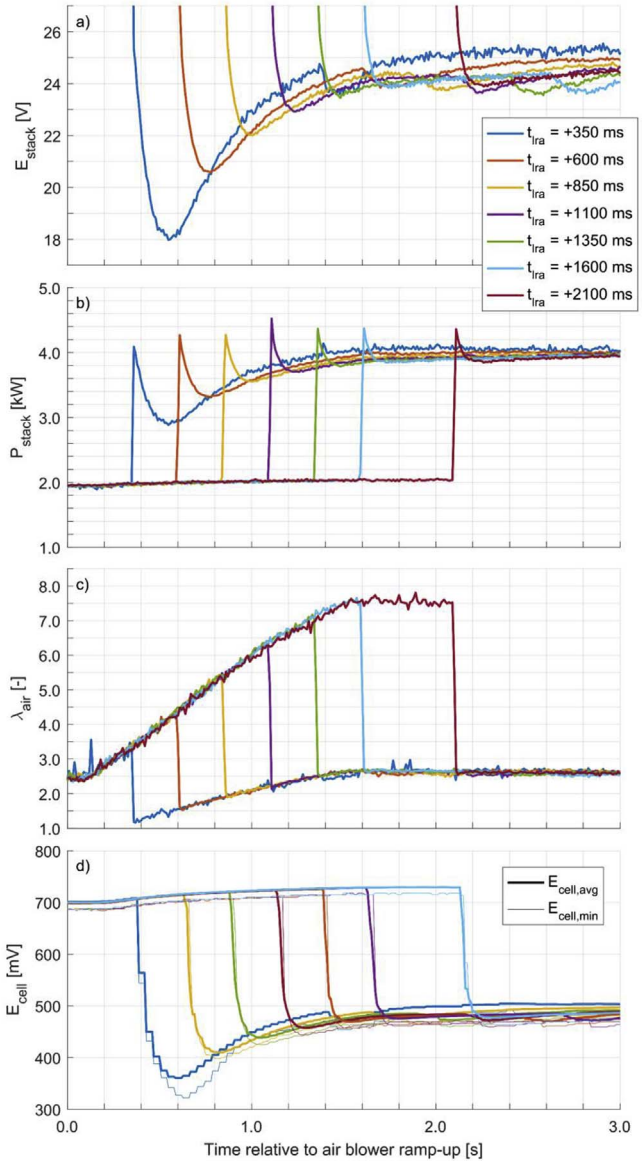

Fig. 7. a) Stack voltage (E_{stack}), b) stack power (P_{stack}), c) air stoichiometry (λ_{air}), and d) average and minimum cell voltage ($E_{cell,avg}$, $E_{cell,min}$) during transients with varying load ramp-up timing relative to air blower ramp-up (t_{lra} = +350 ms … +2100 ms).

emergency stop. Upon decreasing the load ramp-up timing relative to the air blower ramp-up to +350 ms, a clear decrease in lowest cell voltage compared to average cell voltage can be observed (Fig. 7d). The cell voltages were measured with a CVM operating at 25 Hz read frequency – hence the roughly 40 ms delay in the readings. A very short voltage dip due to limited air supply does not cause catalyst support degradation, but if the limitation is on fuel supply, catalyst support degradation may occur, as shown by Enz et al. [25].

3.3.2. Varying initial air stoichiometry for a 0.2 s response

Running the system with an initial air stoichiometry ($\lambda_{air,0}$) of 2.5 cannot achieve the 55 A–160 A current ramp in 0.1 s (as 0.1 s was reserved for data transfer etc.). To achieve such a rapid current ramp, the system must be operated with a higher initial air stoichiometry. Fig. 8 shows the results with varying the initial air stoichiometry and the load ramp-up time relative to air blower ramp-up (t_{lra}) fixed at +100 ms.

To achieve a power ramp from 2 kW to 3.7 kW in 0.1 s, an initial air stoichiometry of 7.0 is needed (Fig. 8b). With an initial air stoichiometry of 5.2, a power ramp to 3.5 kW is achieved, which corresponds to

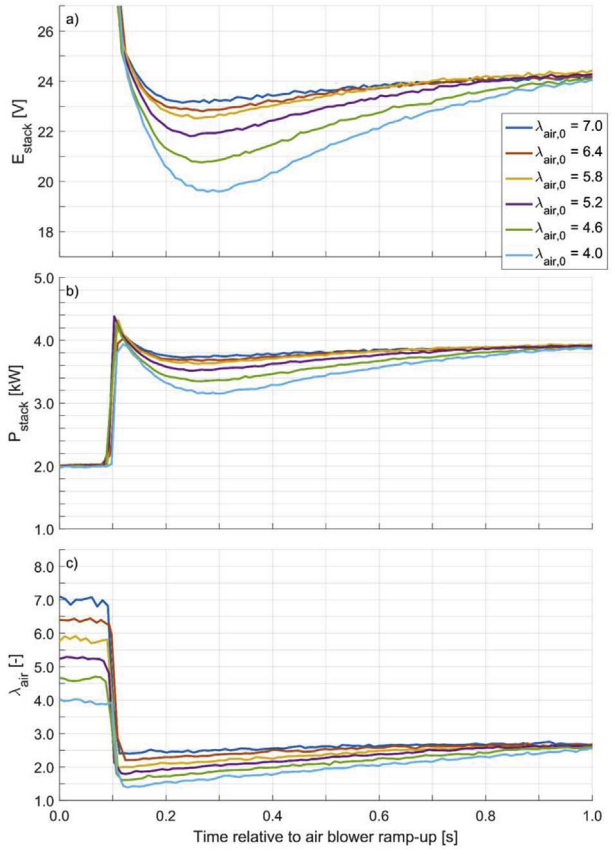

Fig. 8. a) Stack voltage (E_{stack}), b) stack power (P_{stack}), and c) air stoichiometry (λ_{air}) during transients with varying initial air stoichiometry ($\lambda_{air,0}$ = 4.0 … 7.0). Time relative to air blower ramp-up.

a 38% power increase relative to maximum system power. With an initial air stoichiometry of 4.0, the voltage drop is remarkable (Fig. 8a) and a power ramp to only 3.2 kW is achieved because of the low minimum air stoichiometry 1.4 (Fig. 8c).

A high air stoichiometry leads to decreased system efficiency because of air blower power consumption. Further, if a membrane humidifier is employed for air humidification, it should be over-dimensioned. These drawbacks must be evaluated against the benefits from the ancillary services when maximizing the power increase step.

4. Conclusions

The power ramp rate capabilities of a 5 kW PEMFC system using a fixed-geometry ejector with a discrete control solution was studied. The experimental results show that the stack power can be ramped up from 2.0 kW to 4.0 kW (maximum stack power with the current setup) within 0.1 s without problems in fuel supply, even when no mitigation method is applied to dampen the anode pressure fluctuation. Modeling results indicate that if the anode gas volume was reduced by 80%, the anode pressure fluctuation during a similar power ramp could be maintained within 120 mbar. In conclusion, the fuel supply based on ejector with a discrete control does not limit the power ramp rate in the current PEMFC system or in volume-optimized systems.

In the studied system, the air supply limits the power ramp rate because of the slow accelerating air blower. A stack power increase from 2.0 kW to 3.7 kW was achieved in less than 1 s with an initial air stoichiometry of 2.5. A power ramp-up executed earlier results generally in a higher ancillary power capacity even though the encountered low air stoichiometry causes a deep power dip initially. The higher power after the dip is believed to be a consequence of water generation and increased membrane humidity.

When a power ramp from 2.0 kW to 3.7 kW was needed within 0.1 s, an initial stoichiometry of at least 7.0 was necessary. This high air stoichiometry not only consumes much parasitic power, thus lowering the ancillary power capacity of the system, but also necessitates the use of very efficient air humidification to prevent PEMFC dehydration. Therefore, to further increase the power ramp rate capability, additional improvements to the air supply are needed.

Acknowledgements

This work has been supported by the Strategic Research Council at the Academy of Finland, project Transition to a Resource Efficient and Climate Neutral Electricity System (EL-TRAN) (2015–17)" (no. 293437).

This research has received funding from the European Union's Seventh Framework Programme (FP7/2007–2013) for the Fuel Cells and Hydrogen Joint Technology Initiative under grant agreement n° 621218.

Glossary

Latin

E	Voltage, [V]
F	Flow rate, [slpm]
I	Current, [A]
P	Power, [kW]
p	Pressure, [bar]
T	Temperature, [°C]
t	Time, [s]
t_{lra}	Load ramp-up time relative to air blower ramp-up, [s]
t_{lrf}	Load ramp-up time relative to fuel supply ramp-up, [s]

Greek

λ	Stoichiometry [−]

Subscripts

0	Initial
an	Anode
cat	Cathode
in	inlet
min	Minimum
p	Ejector primary inlet

Abbreviations

EFR	Enhanced Frequency Response
FCR-D	Frequency containment disturbance reserves
HVDC	High Voltage Direct Current
lpm	Liters Per Minute
OL3	Olkiluoto 3 nuclear power plant
PEMFC	Proton Exchange Membrane Fuel Cell
PPM	Power Park Module
PV	Photo Voltaic
RoCoF	Rate of Change of Frequency
slpm	Standard Liters Per Minute (T = 293.15 K, p = 1.01325 bara)
TSO	Transmission System Operator
VRE	Variable Renewable Energy

References

[1] P. Tielens, D. Van Hertem, The relevance of inertia in power systems, Renew. Sustain. Energy Rev. 55 (2016) 999–1009, http://dx.doi.org/10.1016/j.rser.2015.11.016.

[2] Nordic TSOs, Challenges and opportunities for the nordic power system, http://www.statnett.no/Global/Dokumenter/Challenges_and_opportunities_Report.pdf, (2016).

[3] European Union, Commission regulation (EU) 2016/631, 68 (2016) 27.04.2016.

[4] ENTSO-E, Need for Synthetic Inertia (SI) for Frequency Regulation - ENTSO-e Guidance Document for National Implementation for Network Codes on Grid Connection, (2017).

[5] ENTSO-E, Nordic balancing philosophy, https://www.entsoe.eu/Documents/Publications/SOC/Nordic/Nordic_Balancing_Philosophy_160616_Final_external.pdf, (2016).

[6] National Grid, Enhanced Frequency Response: Invitation to Tender for Pre-qualified Parties, (2016).

[7] AEMC, System security market frameworks review executive summary system security work program, http://www.aemc.gov.au/getattachment/f510069a-791b-4e4d-8bc0-9e6a216be7a2/Final-report.aspx, (2017) , Accessed date: 28 August 2017.

[8] J. Matevosyan, S. Sharma, S.-H. Huang, D. Woodfin, K. Ragsdale, S. Moorty, P. Wattles, W. Li, Proposed future ancillary services in electric reliability Council of Texas, 2015 IEEE Eindhoven PowerTech, IEEE, 2015, pp. 1–6, , http://dx.doi.org/10.1109/PTC.2015.7232743.

[9] J. Ihonen, Value chain analysis of hydrogen in Finland, http://hdl.handle.net/11250/276892, (2013) , Accessed date: 28 August 2017.

[10] J. Ihonen, P. Koski, V. Pulkkinen, T. Keränen, H. Karimäki, S. Auvinen, K. Nikiforow, M. Kotisaari, H. Tuiskula, J. Viitakangas, Operational experiences of PEMFC pilot plant using low grade hydrogen from sodium chlorate production process, Int. J. Hydrogen Energy 42 (2017) 27269–27283, http://dx.doi.org/10.1016/j.ijhydene.2017.09.056.

[11] P. Corbo, F. Migliardini, O. Veneri, Experimental analysis of a 20 kWe PEM fuel cell system in dynamic conditions representative of automotive applications, Energy Convers. Manag. 49 (2008) 2688–2697, http://dx.doi.org/10.1016/j.enconman.2008.04.001.

[12] P. Corbo, F. Migliardini, O. Veneri, Dynamic behaviour of hydrogen fuel cells for automotive application, Renew. Energy 34 (2009) 1955–1961, http://dx.doi.org/10.1016/j.renene.2008.12.021.

[13] M.A. Danzer, J. Wilhelm, H. Aschemann, E.P. Hofer, Model-based control of cathode pressure and oxygen excess ratio of a PEM fuel cell system, J. Power Sources 176 (2008) 515–522, http://dx.doi.org/10.1016/j.jpowsour.2007.08.049.

[14] I. Matraji, S. Laghrouche, S. Jemei, M. Wack, Robust control of the PEM fuel cell air-feed system via sub-optimal second order sliding mode, Appl. Energy 104 (2013) 945–957, http://dx.doi.org/10.1016/j.apenergy.2012.12.012.

[15] K. Nikiforow, P. Koski, J. Ihonen, Discrete ejector control solution design, characterization, and verification in a 5 kW PEMFC system, Int. J. Hydrogen Energy (2017), http://dx.doi.org/10.1016/j.ijhydene.2017.05.151.

[16] D. Jenssen, O. Berger, U. Krewer, Improved PEM fuel cell system operation with cascaded stack and ejector-based recirculation, Appl. Energy 195 (2017) 324–333, http://dx.doi.org/10.1016/j.apenergy.2017.03.002.

[17] F. Migliardini, T.M. Di Palma, M.F. Gaele, P. Corbo, Hydrogen purge and reactant feeding strategies in self-humidified PEM fuel cell systems, Int. J. Hydrogen Energy 42 (2017) 1758–1765, http://dx.doi.org/10.1016/j.ijhydene.2016.06.196.

[18] A. Martin, L. Jörissen, AutoStack – core – Industry led European consortium to develop next generation automotive stack hardware, 69 (2015) 325335, , http://dx.doi.org/10.1149/06917.0957ecst.

[19] R. Banerjee, S.G. Kandlikar, Two-phase flow and thermal transients in proton exchange membrane fuel cells - a critical review, Int. J. Hydrogen Energy 40 (2015) 3990–4010, http://dx.doi.org/10.1016/j.ijhydene.2015.01.126.

[20] P. Pei, H. Chen, Main factors affecting the lifetime of Proton Exchange Membrane fuel cells in vehicle applications: a review, Appl. Energy 125 (2014) 60–75, http://dx.doi.org/10.1016/j.apenergy.2014.03.048.

[21] J. Dillet, D. Spernjak, A. Lamibrac, G. Maranzana, R. Mukundan, J. Fairweather, S. Didierjean, R.L. Borup, O. Lottin, Impact of flow rates and electrode specifications on degradations during repeated startups and shutdowns in polymer-electrolyte membrane fuel cells, J. Power Sources 250 (2014) 68–79, http://dx.doi.org/10.1016/j.jpowsour.2013.10.141.

[22] R. Borup, J. Meyers, B. Pivovar, Y.S. Kim, R. Mukundan, N. Garland, D. Myers, M. Wilson, F. Garzon, D. Wood, P. Zelenay, K. More, K. Stroh, T. Zawodzinski, J. Boncella, J.E. Mcgrath, M. Inaba, K. Miyatake, M. Hori, K. Ota, Z. Ogumi, S. Miyata, A. Nishikata, Z. Siroma, Y. Uchimoto, K. Yasuda, K.-I. Kimijima, N. Iwashita, Scientific aspects of polymer electrolyte fuel cell durability and degradation, Chem. Rev. 107 (2007) 3904–3951, http://dx.doi.org/10.1021/cr050182l.

[23] K. Nikiforow, P. Koski, H. Karimäki, J. Ihonen, V. Alopaeus, Designing a hydrogen gas ejector for 5 kW stationary PEMFC system – CFD-modeling and experimental validation, Int. J. Hydrogen Energy 41 (2016) 14952–14970, http://dx.doi.org/10.1016/j.ijhydene.2016.06.122.

[24] PowerCell Ab, PowerCell S2 Datasheet, n.d. http://www.powercell.se/wp-content/uploads/2017/05/S2-Data-Sheet.pdf (Accessed 28 August 2017).

[25] S. Enz, T.A. Dao, M. Messerschmidt, J. Scholta, Investigation of degradation effects in polymer electrolyte fuel cells under automotive-related operating conditions, J. Power Sources 274 (2015) 521–535, http://dx.doi.org/10.1016/j.jpowsour.2014.10.127.